Experimental Application of Global Fast Terminal Sliding Mode Controller to TITO System

M. G. Ghogare[1†], **S. L. Patil**[1], **C. Y. Patil**[1], and **L. R. Chaudhari**[2], Non-members

ABSTRACT

Comprehensive analysis of a global fast terminal sliding mode control strategy (GFTSMC) for the multivariable laboratory level control system is presented in this paper. The performance of conventional sliding mode controller strategies experiences chattering as switching control input contains the sgn' function and singularity issues. Moreover, the performance is degraded due to parametric uncertainties and external disturbances. Robustness issues are not well defined in conventional strategies. Global fast terminals remove the chattering effect and eliminate the singularity problem. It has a shorter convergence time and better reaching precision. It shows the finite-time convergence of output variables to the command input. Indirect stability is guaranteed using the direct Lyapunov function. To elicit the performance of the proposed strategy, simulation tests have been conducted on the wood-berry distillation process, while the experimental tests are carried out on a laboratory multivariable process control system. The performance of the proposed strategy is compared to that of conventional sliding mode control and fast terminal sliding mode control.

Keywords: Global fast terminal sliding mode controller, Conventional sliding mode control, Multi-input, Multi-output process, Integral errors, Real-time experimentation

1. INTRODUCTION

Different control strategies have been proposed for controlling multivariable processes. The two-input, two-output (TITO) process is one of the multivariable processes. A decentralized structure is commonly used for TITO processes due to its simpler design and minimum interaction between the state variables of the system [1]. Various nonlinear control strategies have been proposed for better tracking performance, which include adaptive control [2], predictive control [3], fuzzy control [4], and sliding mode control (SMC) [5]. SMC has gained popularity due to its easy, straight-forward implementation, robustness, and fast response [6]. But the chattering phenomenon is inevitable in conventional SMC [7]. System components may get damaged, and the system's performance is hampered due to chattering. Also, the error will not well converge to zero in a finite time in the case of SMC [8].

The high-order sliding mode control or the nonsingular terminal sliding mode control (NSTSMC) could resolve the problem. However, the respective defects of the two methods are obvious. Such as, the high-order sliding mode control could not be applied to the first-order system, and the reaching law of the non-singular terminal sliding mode control is slow when the state of the system is close to the sliding mode surface. Another method to overcome the drawbacks of conventional SMC, the terminal sliding mode controller, was proposed [9]. The surface in terminal sliding mode control (TSMC) is a nonlinear one, but the finite-time convergence can be guaranteed. The performance of closed-loop systems is improved by TSMC in comparison with SMC [11, 12]. A discontinuous term present in TSMC has the chattering effect, and it cannot be completely eliminated. TSMC also suffers from the singularity problem. The speed of convergence cannot be maintained as the states get disturbed, which are located away from the equilibrium point in TSMC [13]. An advanced structure of TSMC, fast TSMC (FTSMC), is proposed to overcome the above issues [14]. With FTSMC, the chattering effect can be eliminated, and the system states perform better for a closed loop system [15]. To improve the phase elimination problem in FTSMC and to remove the chattering, a global sliding mode controller (GSMC) method was proposed in combination with FTSMC. By adding an extra term in the sliding mode surface, GSMC performs better and gives the superior robustness performance [16]. The combination of FTSMC and GSMC, namely global fast terminal sliding mode control (GFTSMC), provides faster convergence to an equilibrium point in a finite time, and by eliminating the reaching phase, system performance is improved [13].

In this paper, a decentralized GFTSMC controller has been proposed for a multivariable process. By implementing the proposed controller, the convergence time, settling time, and rise time have been improved. The wood-berry distillation column problem is presented to check the efficacy of the GFTSMC controller with simulation. A controller is implemented on the level tank system, which is a multivariable process, to validate the performance. With the design of a decentralized

Manuscript received on February 20, 2022; revised on August 23, 2022; accepted on December 1, 2022. This paper was recommended by Associate Editor Matheepot Phattanasak.

[1]The author is with College of Engineering Pune, India,

[2]The author is with Dr. D. Y. Patil Institute of Technology, Pune, India,

[†]Corresponding author: mukeshgghogare@gmail.com

Digital Object Identifier: 10.37936/ecti-eec.2023212.249727

GFTSMC controller with a decoupler, the coupling effect in the multi-input, multi-output (MIMO) system can be eliminated. With the help of decouplers, the interactions between the variables are minimized, and for each system, a decoupled subsystem is formed. An independent GFTSMC controller is designed for each decoupled system separately, and the system response is analyzed.

The paper is organized as follows: The next section presents a brief study of GFTSMC design with stability analysis. Section 3 gives a brief description of the MIMO system and its modeling. The simulation test on the wood-berry distillation column with GFTSMC is presented in Section 4. Section 5 is devoted to real-time experimentation with the results of the proposed controller. Finally, a work summary has been presented.

2. GLOBAL-FAST TERMINAL SLIDING MODE CONTROL

2.1 Problem formulation

Consider a nonlinear system given by Eq. (1) [17-19],

$$\begin{aligned} \dot{x}_1(t) &= x_2(t) \\ \dot{x}_2(t) &= a(x,t) + b(x,t)u(t) + d(x,t) \\ y(t) &= x_1(t) \end{aligned} \tag{1}$$

where $x = \begin{bmatrix} x_1 & x_2 \end{bmatrix}^T$, x_1 and x_2 are system states, $a(x,t), b(x,t)$ are smooth functions, $b(x,t) \neq 0, d(t)$ denotes the uncertainties and $|d(t)| \leq L$ denotes the disturbances. d(x,t) is a bounded lump uncertainty in Eq. (1), i.e. $|d(x,t)| \leq D_max$. The aim is to design a GFTSMC such that the state of the system Eq. (1) will converge to an equilibrium point in finite-time so that the control efforts are minimal.

2.2 Controller Design

Global fast terminal sliding surface is given by Eq. (2) [20],

$$s(t) = \dot{e}(t) + \alpha e(t) + \beta e^{q/p} = 0 \tag{2}$$

where $\alpha > 0$, $\beta > 0$, p and q are positive odd numbers, and $p > q$. Based on Eq. (2), a new sliding surface for FTSMC control of higher-order systems is given as

$$\begin{aligned} s_1(t) &= \dot{e}_0(t) + \alpha_0 e_0(t) + \beta_0 e_0(t)^{q_0/p_0} \\ s_2(t) &= \dot{e}_1(t) + \alpha_1 e_1(t) + \beta_1 e_1(t)^{q_1/p_1} \\ &\vdots \\ s_{n-1}(t) &= \dot{e}_{n-2}(t) + \alpha_{n-2} e_{n-2}(t) + \beta_{n-2} e_{n-2}(t)^{q_{n-2}/p_{n-2}} \end{aligned} \tag{3}$$

where n is the order of the system, e_0 is initial error. $\alpha_i, \beta_i > 0$ and p_i,q_i where, $i = 1, 2, \ldots, n-2$, are positive-odd-integers. For $n = 2$, the nonlinear sliding variable [1] is,

$$s(t) = \dot{e}(t) + \alpha e(t) + \beta e(t)^{q/p} \tag{4}$$

where $e(t) = y(t) - y_d(t)$ is the tracking error, $y(t)$ and $y_d(t)$ are actual output and desired output of the system, respectively. In finite-time [13, 21], the error signal, $e(t)$, on a sliding surface reaches its origin, for $e(0) \neq 0$

$$t_s = \frac{p}{\alpha(p-q)} \ln \frac{\beta + \alpha e(0)^{(p-q)/p}}{\beta} \tag{5}$$

By selecting α, β, p, q, the system state attains equilibrium in a finite-time t_s.
From Eq. (4),

$$\dot{e}(t) = -\alpha e(t) - \beta e(t)^{q/p} \tag{6}$$

When $e(t)$ is far from the origin, $\dot{e}(t) = -\beta e(t)^{q/p}$, which is a fast terminal attractor, decides the convergent time. When $e(t)$ approaches the origin, convergent time is determined by, $\dot{e}(t) = -\alpha e(t)$. Therefore, the terminal attractor given in Eq. (5) makes the states converge to zero in a finite-time. Also, the speed of a linear sliding surface is guaranteed. The surface in Eq. (4) is a global fast sliding surface.

The global fast sliding surface is selected as

$$s_1(t) = \dot{e}_0(t) + \alpha_0 e_0(t) + \beta_0 e_0(t)^{q_0/p_0} \tag{7}$$

where $\alpha_0, \beta_0 > 0$ and $q_0, p_0 (q_0 < p_0)$ are positive odd numbers. Differentiating the above equation and substituting Eq. (1) leads to,

$$\begin{aligned} \dot{s}_1(t) &= \ddot{e}_0(t) + \alpha_0 \dot{e}_0(t) + \beta_0 \frac{d}{dt} e_0(t)^{q_0/p_0} \\ &= a(x,t) + b(x,t)u(t) + d(t) + \alpha_0 \dot{e}_0(t) + \\ &\beta_0 \frac{d}{dt} e_0(t)^{q_0/p_0} \end{aligned} \tag{8}$$

The GFTSMC is,

$$\begin{aligned} u(t) = &- b(x,t)^{-1}[a(x,t) + \alpha_0 \dot{e}_0(t) + \beta_0 \frac{d}{dt} e_0(t)^{q_0/p_0} + \\ &\phi e_1(t) + \gamma e_1(t)^{q/p}] \end{aligned} \tag{9}$$

where ϕ is the boundary layer thickness and $\gamma > 0$.

2.3 Stability Analysis

The Lyapunov function is selected as Eq. (10) [18, 22],

$$V(t) = \frac{1}{2} s_1(t)^2 \tag{10}$$

Because

$$\begin{aligned} \dot{\hat{s}}_1 = &\quad \hat{e}_0(t) + \alpha_0 \hat{e}_0(t) + \beta_0 \tfrac{d}{dt} e_0(t)^{q_0/p_0} \\ = &\quad a(x,t) + b(x,t)u(t) + d(t) + \alpha_0 \hat{e}_0(t) + \\ &\beta_0 \tfrac{d}{dt} e_0(t)^{q_0/p_0} \end{aligned} \tag{11}$$

Substituting Eq. (9) in Eq. (8),

$$\dot{s}_1(t) = -\phi e_1(t) - \gamma e_1(t)^{q/p} + d(t) \tag{12}$$

Taking derivative of Eq. (10) [23],

$$\begin{aligned} \dot{V}(t) &= s_1(t)\dot{s}_1(t) \\ &= -\phi e_1(t)^2 - \gamma e_1(t)^{(q+p)/p} + e_1(t)d(t) \end{aligned} \tag{13}$$

$(p + q)$ is even because $-\gamma e_1(t)^{(q+p)/p} + e_1 d(t) \leq 0$ is satisfied and $\gamma \geq \left|\frac{1}{e_1(t)^{q/p}}\right| |d(t)|$ or $\gamma \geq \left|\frac{1}{e_1(t)^{q/p}}\right| L$, therefore $\dot{V}(t) \leq 0$.

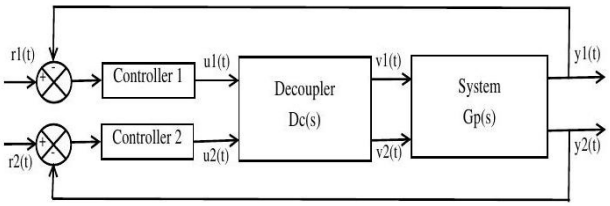

***Fig. 1**: Block diagram of decentralized controller.*

2.4 Position Control

Let the desired point be y_d, also $e_0 = y_1 - y_d$ therefore, $\dot{e}_0(t) = \dot{y}_1 - \dot{y}_d$ and $\ddot{e}_0(t) = \ddot{y}_1 - \ddot{y}_d$. Eq. (8) can be rewritten as

$$\begin{aligned} \dot{s}_1(t) &= \ddot{e}_0(t) + \alpha_0 \dot{e}_0(t) + \beta_0 \frac{d}{dt} e_0(t)^{q_0/p_0} \\ &= a(x,t) + b(x,t)u(t) + d(t) - \ddot{y}_d + \alpha_0 \dot{e}_0(t) + \\ &\beta_0 \frac{d}{dt} e_0(t)^{q_0/p_0} \end{aligned} \tag{14}$$

The controller given by Eq.(9) can be written in modified form as

$$\begin{aligned} u(t) = &- b(x,t)^{-1}[a(x,t) - \ddot{y}_d + \alpha_0 \dot{e}_0(t) + \beta_0 \frac{d}{dt} e_0(t)^{q_0/p_0} + \\ &\phi e_1(t) + \gamma e_1(t)^{q/p}] \end{aligned} \tag{15}$$

3. MIMO SYSTEM

Fig. 1 shows a MIMO linear system with decoupler. $G_p(s)$,$D_c(s)$ are the plant and decoupler respectively. Then,

$$G_p(s) = \begin{bmatrix} G_{p_{11}}(s) & G_{p_{12}}(s) & \dots & G_{p_{1m}}(s) \\ G_{p_{21}}(s) & G_{p_{22}}(s) & \dots & G_{p_{2m}}(s) \\ \vdots & \vdots & \vdots & \vdots \\ G_{p_{m1}}(s) & G_{p_{m_2}}(s) & \dots & G_{p_{mm}}(s) \end{bmatrix} \tag{16}$$

and

$$D_c(s) = \begin{bmatrix} D_{c_{11}}(s) & D_{c_{12}}(s) & \dots & D_{c_{1m}}(s) \\ D_{c_{21}}(s) & D_{c_{22}}(s) & \dots & D_{c_{2m}}(s) \\ \vdots & \vdots & \vdots & \vdots \\ D_{c_{m1}}(s) & D_{c_{m2}}(s) & \dots & D_{c_{mm}}(s) \end{bmatrix} \tag{17}$$

The multiloop SISO structure is,

$$F(s) = G_p(s) D_c(s) \tag{18}$$

where $F(s)$ is a diagonal matrix represented by,

$$F(s) = \begin{bmatrix} F_{11}(s) & 0 & \cdots & 0 \\ 0 & F_{22}(s) & \cdots & 0 \\ \vdots & \vdots & \vdots & \vdots \\ 0 & 0 & \cdots & F_{mm}(s) \end{bmatrix} \tag{19}$$

From Eq. (18), decoupler can be given as

$$D_e(s) = Adj\left[G_p(s)\right] Q(s) \tag{20}$$

where $Q(s)$= diagonal matrix. From Eq. (16), two decoupled subsystems are obtained. $F_{11}(s)$ and $F_{22}(s)$ are the second-order structure of the MIMO linear system. The state-space representation of these subsystems is represented as

$$\begin{aligned} \dot{x}_1(t) &= x_2(t) \\ \dot{x}_2(t) &= a_1(x,t) + b_1(x,t)u_1(t) + d_1(x,t) \\ y_1(t) &= x_1(t) \\ \dot{x}_3(t) &= x_4(t) \\ \dot{x}_4(t) &= a_2(x,t) + b_2(x,t)u_2(t) + d_2(x,t) \\ y_2(t) &= x_3(t) \end{aligned} \tag{21}$$

where $x = \left[x_1, x_2, x_3, x_4\right]^T$ is the state vector, a_1, a_2, b_1, and b_2 are nonlinear functions. u_1 and u_2 are the control inputs. The lumped uncertainties $d_1(x,t) = \Delta a_1(x,t) + \Delta b_1(x,t)u_1(t) + \delta_1(x,t)$ and $d_2(x,t) = \Delta a_2(x,t) + \Delta b_2(x,t)u_2(t) + \delta_2(x,t)$ are assumed to be bounded as $d_1(x,t) \le D_{max1}, d_2(x,t) \le D_{max2}$.

The Eqs. (18) and (19) represent two decoupled subsystems, where the controlled variables are y_1 and y_2. Using sliding surfaces, the decentralized control is implemented as

$$\begin{aligned} s_1(t) &= \dot{e}_1(t) + \alpha_1 e_1(t) + \beta_1 e_1(t)^{q_1/p_1} \\ s_2(t) &= \dot{e}_2(t) + \alpha_2 e_2(t) + \beta_2 e_2(t)^{q_2/p_2} \end{aligned} \tag{22}$$

where $e_1 = y_1 - y_{d1}; e_2 = y_2 - y_{d2}; \alpha_1, \alpha_2, \beta_1, \beta_2 > 0; q_1 < p_1$ and $q_2 < p_2$ are odd positive integers. The control laws explained in Section 2.2 for two decoupled subsystems can be given as,

$$\begin{aligned} u_1(t) = &- b_1(x,t)^{-1}[a_1(x,t) + \alpha_1 \dot{e}_1(t) + \beta_1 \frac{d}{dt} e_1(t)^{q_1/p_1} + \\ &\phi_1 e_1(t) + \gamma_1 e_1(t)^{q_1/p_1}] \\ u_2(t) = &- b_2(x,t)^{-1}[a_2(x,t) + \alpha_2 \dot{e}_2(t) + \beta_2 \frac{d}{dt} e_2(t)^{q_2/p_2} + \\ &\phi_2 e_2(t) + \gamma_2 e_2(t)^{q_2/p_2}] \end{aligned} \tag{23}$$

where $\gamma_1 \ge \left|\frac{1}{e_1(t)^{q_1/p_1}}\right| L_1$ and $\gamma_2 \ge \left|\frac{1}{e_2(t)^{q_2/p_2}}\right| L_2$.

The stability discussed in [23,24] is proved in Section 2.3. and can be applied for MIMO system.

4. SIMULATION RESULTS

To check the efficacy of the proposed controller, a Wood-Berry binary distillation column example is used for simulation. The process transfer function matrix can be given as Eq. (24) [25],

$$G_{WB_p}(s) = \begin{bmatrix} \frac{12.8e^{-s}}{1+16.734s} & \frac{-18.9e^{-3s}}{1+21.019s} \\ \frac{6.6e^{-7s}}{1+10.9052s} & \frac{-19.4e^{-3s}}{1+14.405s} \end{bmatrix} \tag{24}$$

For design, the ideal decoupler is chosen as

$$D_{WB_C}(s) = Adj\left[G_{WB_p}(s)\right] Q(s) \tag{25}$$

where $Q(s)$ is a diagonal matrix. The common pole-zero, common dead time, and smallest gain from i^{th} column of $Adj\left[G_{WBp}(s)\right]$ are removed for obtaining the elements of the $Q(s)\left(k_i(s)\right)$. From Eq. (24), the decoupler can be given Eq. (26) as

$$D_{WB_c}(s) = \begin{bmatrix} D_{11}(s) & D_{12}(s) \\ D_{21}(s) & D_{22}(s) \end{bmatrix} \tag{26}$$

where $D_{11}(s) = \frac{2.9347}{1+14.402s}, D_{12}(s) = \frac{1.477e^{-2s}}{1+21.019s}, D_{21} = \frac{e^{-4s}}{1+10.9052s}$, and $D_{22}(s) = \frac{1}{1+16.734s}$.

From Eq. (16),

$$\begin{aligned} F(s) =& G_{WB_p}(s) D_{WB_c}(s) \\ F_{11}(s) =& \frac{37.63e^{-s}}{(1+16.734s)(1+14.402s)} - \\ & \frac{18.9e^{-7s}}{(1+21.019s)(1+14.402s)} \\ F_{12}(s) =& F_{21}(s) = 0 \end{aligned} \tag{27}$$

and

$$\begin{aligned} F_{22}(s) =& \frac{9.75e^{-9s}}{(1+10.9052s)(1+21.019s)} - \\ & \frac{19.4e^{-3s}}{(1+14.402s)(1+16.734s)} \end{aligned} \tag{28}$$

where $F_{11}(s)$ and $F_{22}(s)$ are of higher order. The frequency response fitting method at two points is used to obtain the first-order system plus dead-time (FOPDT) model. The two frequencies are given by Eq. (29),

$$\begin{aligned} G_i(0) &= F_i(0) \\ \left|G_i\left(j\omega_{ci}\right)\right| &= \left|F_i\left(j\omega_{ci}\right)\right| \\ \angle G_i\left(j\omega_{ci}\right) &= \angle F_i\left(j\omega_{ci}\right) \end{aligned} \tag{29}$$

given $\omega = 0$ and $\omega = \omega_{cf}$, where ω_{cf} is phase crossover frequency [26]. From the above result, FOPDT model parameters are calculated as Eq. (30) [27]

$$\begin{aligned} K_i &= F_i(0) \\ T_i &= \sqrt{\frac{K_i^2 - \left|F_i\left(j\omega_{cf}\right)\right|^2}{\left|F_i\left(j\omega_{cf}\right)\right|^2 \omega_{cf}^2}} \\ \tau_i &= \frac{\pi + \tan^{-1}\left(-\omega_{cf} T_i\right)}{\omega_{cf} T_i} \end{aligned} \tag{30}$$

Using Eqs. (28) and (29) the FOPDT model can be represented as

$$G_{i_{FOPDT}}(s) = \frac{K_i e^{-\tau_i s}}{T_i s + 1}, i = 1, 2 \tag{31}$$

Using Eq. (30), the FOPDT subsystems are

$$\begin{aligned} G_{11_{FOPDT}} &= \frac{18.73e^{-3.45s}}{1+68.24s} \\ G_{22_{FOPDT}} &= \frac{-9.65e^{-6.47s}}{1+52.38s} \end{aligned} \tag{32}$$

Using Taylor series approximation, the delayed term in Eq. (30) is given as

$$e^{-\tau_i s} = \frac{1}{1+\tau_i s} \tag{33}$$

The FOPDT subsystems are,

$$\begin{aligned} G_{11_{re}} &= \frac{18.73}{(1+68.24s)(1+3.45s)} \\ G_{22_{re}} &= \frac{-9.65}{(1+52.38s)(1+6.47s)} \end{aligned} \tag{34}$$

Eqs. (22) and (23) gives the two separate GFTSMC decoupled systems,

$$\begin{aligned} u_1(t) =& -0.0045y_1 - (0.3017+\alpha_1)\dot{y}_1 - \beta_1 \frac{d}{dt} e_1(t)^{(q_1/p_1)} + \\ & \alpha_1 \dot{y}_{d1} + \ddot{y}_{d1} - \phi_1 e_1(t) - \gamma_1 e_1(t)^{(q_1/p_1)} \\ u_2(t) =& -0.0032y_2 - (0.1763+\alpha_2)\dot{y}_2 - \beta_2 \frac{d}{dt} e_2(t)^{(q_2/p_2)} + \\ & \alpha_2 \dot{y}_{d2} + \ddot{y}_{d2} - \phi_2 e_2(t) - \gamma_2 e_2(t)^{(q_2/p_2)} \end{aligned} \tag{35}$$

where

$$\begin{aligned} s_1(t) &= \dot{e}_1(t) + \alpha_1 e_1(t) + \beta_1 e_1(t)^{q_1/p_1} \\ s_2(t) &= \dot{e}_2(t) + \alpha_2 e_2(t) + \beta_2 e_2(t)^{q_2/p_2} \end{aligned} \tag{36}$$

For simulation studies, values of the constants in Eqs. (34) and (35) are taken as, $\alpha_1 = 1.347, \alpha_2 = 1.6132, \beta_1 = 0.5167, \beta_2 = 0.834, \phi_1 = 0.0149, \phi_2 = 0.0276, L_1 = 0.832, L_2 = 0.9637$, and $y_{d1} = y_{d2} = 1$.

From Eqs. (32) and (33), the control signals, $u_1(t)$ and $u_2(t)$ are designed such that they are used to track the given setpoint, for the wood-berry distillation column. A numerical simulation using MATLAB/Simulink platform is carried out. Figs. 2 and 3 show the results for setpoint tracking and controller efforts without any disturbances. The GFTSMC controller performs better than the other strategies. Figs. 4 and 5 show the result of a multi-level setpoint change and the disturbances to check the robustness of the controller. Table 1. gives the summary

***Table 1**: Summary of simulation results: M_p, peak overshoot (%); t_r, rise time(sec); t_s, settling time; ISE, integral square error; IAE, integral absolute error.*

Controller Type	M_p	t_r	t_s	ISE	IAE
GFTSMS	0	4.35	32.9	48.6	83.10
FTSMS	0	5.01	41.23	50.67	88.79
SMC	0	6.26	55.2	53.25	91.27

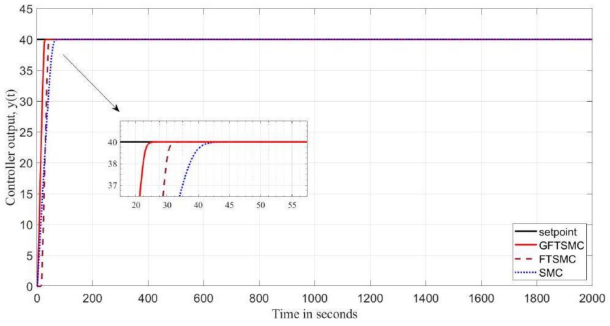

***Fig. 2**: Output response without disturbances.*

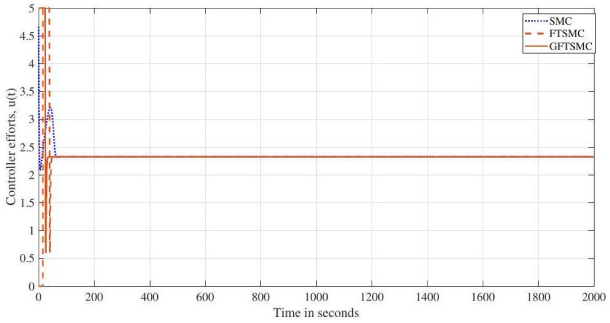

***Fig. 3**: Controller efforts.*

of simulation results for time-domain specifications and performance indices such as integral square error (ISE) and integral absolute error (IAE).

To check the robustness of the proposed controller, 0.5% of external disturbances are added at 800 and 1500 seconds with 15% parametric uncertainty in the system model. Similarly, the setpoint is changed from 40% to 50% for 600 to 1000 seconds and 40% to 34% from 1400 to 1700 seconds. From Figs. 4 and 5, it is observed that the suggested controller rejects external disturbances and setpoint changes.

5. EXPERIMENTAL WORK

5.1 System Modeling

Experimental tests are conducted on a nonlinearly coupled tank level system to check the applicability and efficiency of the proposed method. Fig. 6 shows, laboratory experimental setup. An adjustable valve (V_1) is used to interlink the coupled tanks. Control valve V_2 and V_3 are provided for discharge. Each tank has a level transmitter (LT) to have 4-20mA supply output

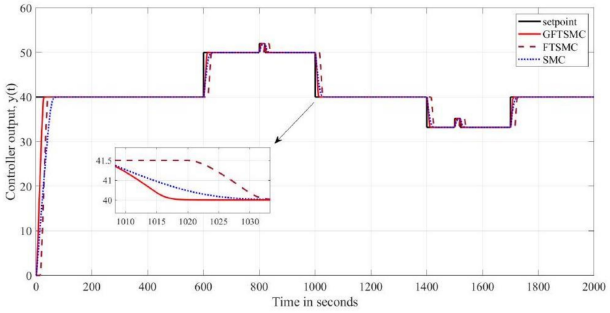

***Fig. 4**: Output response with disturbance and multilevel setpoint change with 15% parametric uncertainty.*

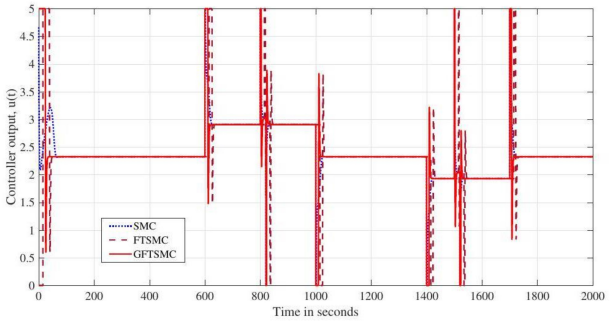

***Fig. 5**: Controller efforts with disturbance and multilevel setpoint change with 15% parametric uncertainty.*

***Fig. 6**: Laboratory setup.*

equivalent to 0-100% of tank level.

To provide flow in each tank, a positive displacement pump is used. A DAQ card, PCI 6014E, is used for interfacing the system with a personnel computer. Through a current- to-voltage converter, the level transmitter is connected to analog input channel BNC 2120. For variable frequency drives (VFD), the controller signal 0-5V is converted to 4-20mA; through BNC 2120. Using MATLAB and Simulink, the controller algorithm is implemented. By using the system identification method [27], the real-time system's overall transfer function

matrix is,

$$G_T(s) = \begin{bmatrix} \frac{0.43e^{-5s}}{1+29s} & \frac{0.145e^{-10s}}{1+40s} \\ \frac{0.172e^{-10s}}{1+35s} & \frac{0.37e^{-5s}}{1+27s} \end{bmatrix} \tag{37}$$

From Eq. (26), the decoupler is calculated as

$$Adj[G_T(s)] = \begin{bmatrix} \frac{0.37e^{-5s}}{1+27s} & \frac{-0.172e^{-10s}}{1+40s} \\ \frac{-0.145e^{-10s}}{1+35s} & \frac{0.43e^{-5s}}{1+29s} \end{bmatrix} \tag{38}$$

$$K(s) = \begin{bmatrix} \frac{e^{5s}}{0.145} & 0 \\ 0 & \frac{e^{5s}}{0.172} \end{bmatrix} \tag{39}$$

$$D_{e_T}(s) = \begin{bmatrix} \frac{2.55}{1+27s} & \frac{e^{-5s}}{1+40s} \\ \frac{-e^{-5s}}{1+35s} & \frac{2.5}{1+29s} \end{bmatrix} \tag{40}$$

The decoupled subsystems are computed as,

$$\begin{aligned} F_{11}(s) =& \frac{1.0965e^{-5s}}{(1+27s)(1+29s)} - \frac{0.172e^{-15s}}{(1+35s)(1+40s)} \\ F_{12}(s) =& F_{21}(s) = 0 \end{aligned} \tag{41}$$

and

$$F_{22}(s) = \frac{0.925e^{-5s}}{(1+27s)(1+29s)} - \frac{0.145e^{-3s}}{(1+35s)(1+40s)} \tag{42}$$

With delay approximation, the reduced forms of $F_{11}(s)$ and $F_{22}(s)$ are

$$\begin{aligned} G_{11_{re}} &= \frac{0.9245e^{-12.7s}}{(1+113.2s)} \approx \frac{0.9245}{(1+113.2s)(1+12.7s)} \\ G_{22_{re}} &= \frac{0.78e^{-12.7s}}{(1+113.2s)} \approx \frac{0.78}{(1+113.2s)(1+12.7s)} \end{aligned} \tag{43}$$

State models of $G_{11_{re}}$ and $G_{22_{re}}$ are used for obtaining the Control signals u_1 and u_2 as,

$$\begin{aligned} u_1(t) =& -0.0007012y_1 - (0.0967+\alpha_1)\dot{y}_1 - \\ & \beta_1 \frac{d}{dt} e_1(t)^{(q_1/p_1)} + \alpha_1 \dot{y}_{d1} + \\ & \ddot{y}_{d1} - \phi_1 e_1(t) - \gamma_1 e_1(t)^{(q_1/p_1)} \\ u_2(t) =& -0.00065409y_2 - (0.0851+\alpha_2)\dot{y}_2 - \\ & \beta_2 \frac{d}{dt} e_2(t)^{(q_2/p_2)} + \alpha_2 \dot{y}_{d2} + \\ & \ddot{y}_{d2} - \phi_2 e_2(t) - \gamma_2 e_2(t)^{(q_2/p_2)} \end{aligned} \tag{44}$$

Through the decoupler, these control signals are applied to the plant. Results obtained from simulation tests for the proposed controller are validated with real-time experiments conducted on a laboratory setup.

Control law constants in Eqs. (36) and (37) are, $p_1 = p_2 = 9, q_1 = q_2 = 5, \alpha_1 = 2.1057, \alpha_2 = 2.625, \beta_1 = 2.5265, \beta_2 = 2.8614, \phi_1 = 0.1085$, and $\phi_2 = 0.2253$.

***Table 2**: Summary of experimental results for Tank1: M_p, peak overshoot (%); t_r, rise time(sec); t_s, settling time; ISE, integral square error; IAE, integral absolute error.*

Controller Type	M_p	t_r	t_s	ISE	IAE
SMC	0	25.9	73.7	63.75	99.37
GFTSMS	0	25	70	52.38	88.71

***Table 3**: Summary of experimental results for Tank2: M_p, peak overshoot (%); t_r, rise time(sec); t_s, settling time; ISE, integral square error; IAE, integral absolute error.*

Controller Type	M_p	t_r	t_s	ISE	IAE
SMC	0	26.62	86.1	69.53	96.21
GFTSMS	0	26.03	74.7	59.01	90.83

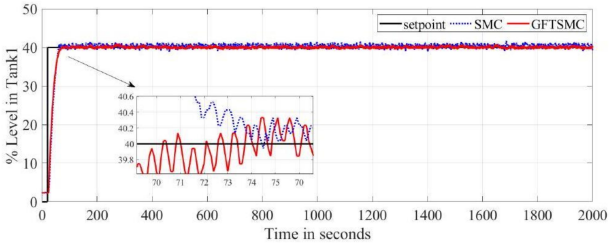

***Fig. 7**: Nominal output response for Tank1.*

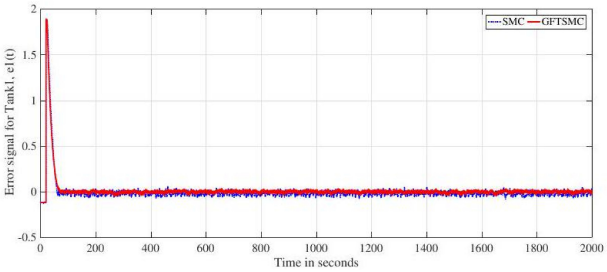

***Fig. 8**: Error signal for Tank1.*

5.2 Experimental Results

Controller outputs, $u_1(t)$ and $u_2(t)$ are designed such that they are used to track the output. An experiment is performed on a coupled tank using MATLAB/Simulink, and results for Tank1 and Tank2 are shown. Figs. 7, 8, 9, and 10 show the setpoint tracking without disturbance, error signal $e_1(t)$, sliding surface $s_1(t)$ and controller efforts $u_1(t)$ respectively, for Tank 1, SMC, and GFTSMC. Similarly, Figs. 11, 12, 13, and 14 show the responses for Tank 2. Tables 2 and 3 give the summary of the experimental results for Tank1 and Tank2 in terms of time domain and performance indices such as ISE and IAE for both controllers.

For testing, the robustness of the controller, setpoint is been changed from 40% to 50% for 600 -1000 seconds and from 50% to 40% for 1000 – 1400 seconds as a step signal. Also, from 1400- 1700 seconds, the setpoint is changed

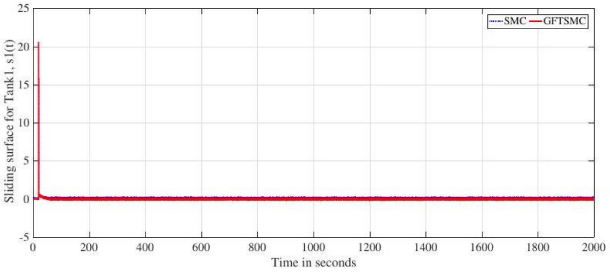

***Fig. 9**: Sliding surface of Tank1.*

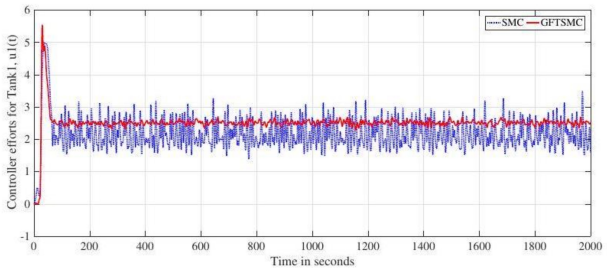

***Fig. 10**: Controller efforts for Tank1.*

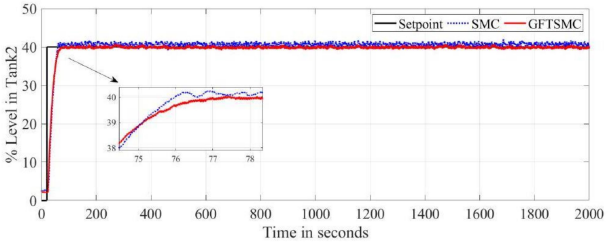

***Fig. 11**: Nominal output response for Tank2.*

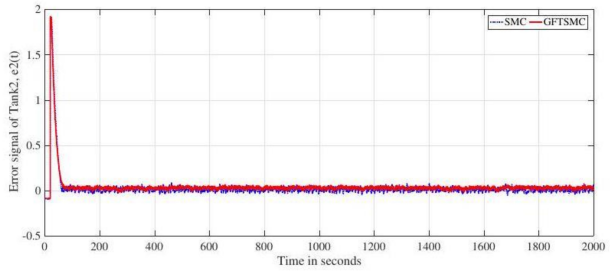

***Fig. 12**: Error signal for Tank2.*

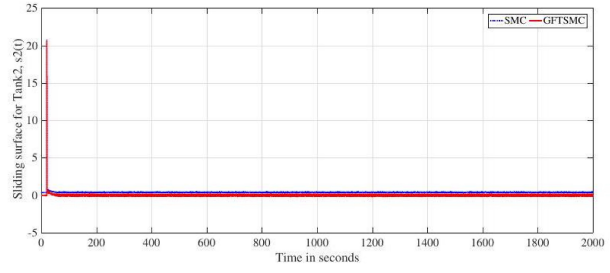

***Fig. 13**: Sliding surface of Tank2.*

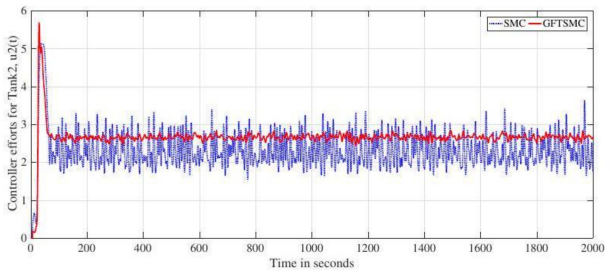

***Fig. 14**: Controller efforts for Tank2.*

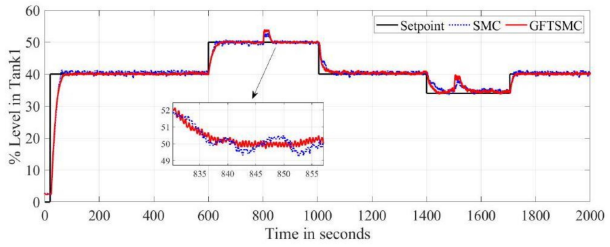

***Fig. 15**: Output response for Tank1 with external disturbances and setpoint change.*

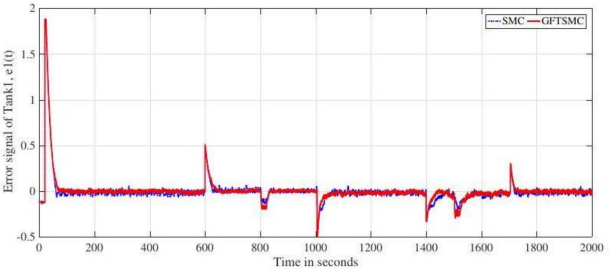

***Fig. 16**: Error signal for Tank1.*

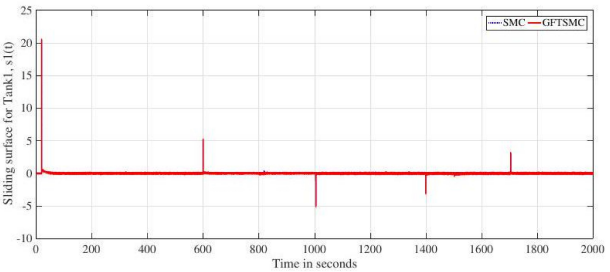

***Fig. 17**: Sliding surface of Tank1.*

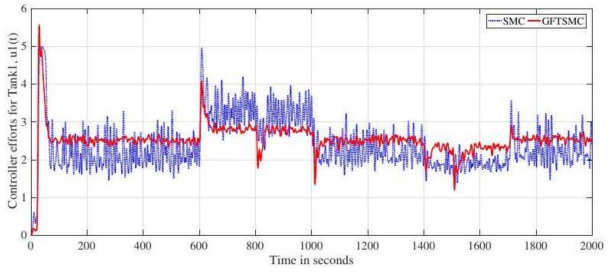

***Fig. 18**: Controller efforts for Tank1.*

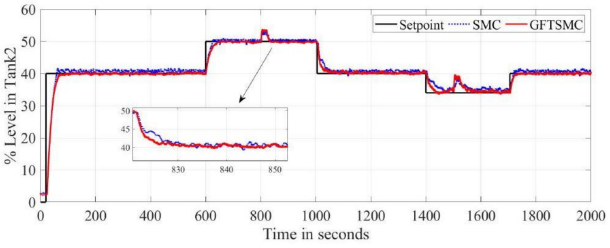

***Fig. 19**: Output response for Tank2 with external disturbances and setpoint change.*

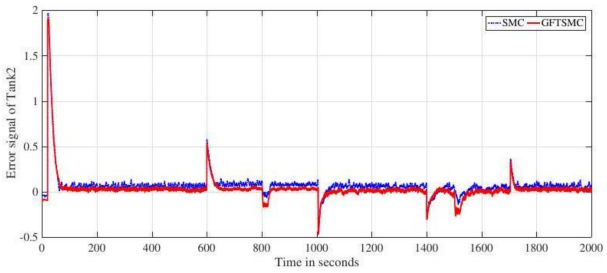

***Fig. 20**: Error signal for Tank2.*

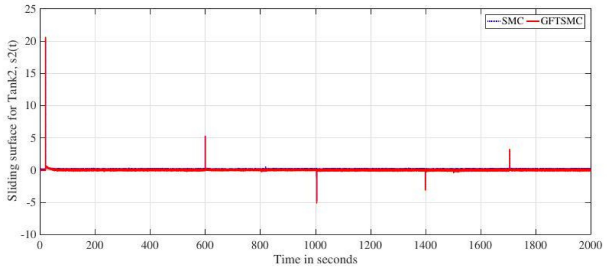

***Fig. 21**: Sliding surface of Tank2.*

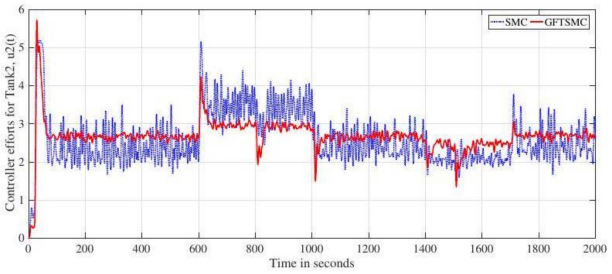

***Fig. 22**: Controller efforts for Tank2.*

from 40% to 34% and from 34% to 40% for 1700 - 2000 seconds for both tanks.

In between, for 20 seconds, a 0.5% disturbance is added from 800- 820 seconds and 1500- 1520 seconds for both tanks. Figs. 15, 16, 17, and 18 show the setpoint tracking with setpoint change and external disturbance added, error signal $e_1(t)$, sliding surface $s_1(t)$ and controller efforts $u_1(t)$ respectively for Tank1, SMC, and GFTSMC. Similarly, Figs. 19, 20, 21, and 22 show the responses for Tank2.

From Figs. 7 and 11, it can be seen that the GFTSMC controller converges rapidly as compared to conventional SMC. The chattering is also minimized using GFTSMC, as can be verified from Figs. 10 and 14. Figs. 15 and 19 show the responses for the proposed controller in Tanks 1 and 2, respectively, for multi-level setpoints and disturbances for checking the robustness of the controller. 0.5% disturbance is added by opening a tap above the two tanks for 20 seconds to disturb the level. 0.5% disturbance means the level is changed from 50% to 52.5% by adding water. From Figs. 15 and 19, the GFTSMC controller performs far better in the presence of setpoint changes and disturbances. Also, from Figs. 18 and 22, it can be seen that, the chattering is minimized. Overall results, show that, the proposed scheme can effectively handle setpoint change and external disturbances.

6. CONCLUSION

In this paper, the GFTSMC method for multivariable processes is analyzed. Based on the developed algorithm, the proposed controller has minimal chattering and a fast convergence time as compared to other control strategies. To validate the performance of the proposed controller, simulation is carried out on a Wood-Berry distillation column, and experimentation is carried out on a nonlinearly coupled tank system. The results were compared with those of conventional SMC and FTSMC. The simulation and experimental results confirm that the proposed controller performs effectively for setpoint tracking, disturbances, and parametric uncertainty. The controller efforts are minimal for GFTSMC as compared to FTSMC and SMC.

REFERENCES

[1] B. J. Parvat and B. M. Patre, "Fast terminal sliding mode controller for square multivariable processes with experimental application," *International Journal of Dynamics and Control*, vol. 5, no. 4, pp. 1139–1146, Jul. 2016.

[2] H. H. Choi, N. T. -T. Vu, and J. -W. Jung, "Digital Implementation of an Adaptive Speed Regulator for a PMSM," *IEEE Transactions on Power Electronics*, vol. 26, no. 1, pp. 3-8, Jan. 2011.

[3] R. Errouissi, M. Ouhrouche, W. -H. Chen, and A. M. Trzynadlowski, "Robust Cascaded Nonlinear Predictive Control of a Permanent Magnet Synchronous Motor With Antiwindup Compensator," *IEEE Transactions on Industrial Electronics*, vol. 59, no. 8, pp. 3078-3088, Aug. 2012.

[4] L. Cui, J. Huang, X. Shi, et al., "Fuzzy logic based variable-order fractional sliding mode control for PMSM," *Journal of Electrical Measurement and Instrumentation*, Vol. 54 No. 6, pp. 81-86, 2017.

[5] Y. Shtessel, C. Edwards, L. Fridman, and A. Levant, *Sliding mode control and observation*. New York: Springer, 2014.

[6] L. Xiang, W. Yan, and J. Zhicheng, "Global Fast Terminal Sliding Mode Control System for Permanent Magnet Synchronous Motor Drive Under Dis-

turbances," in *2018 37th Chinese Control Conference (CCC)*, Wuhan, China, 2018, pp. 3092-3095.

[7] I. González, S. Salazar, and R. Lozano, "Chattering-Free Sliding Mode Altitude Control for a Quad-Rotor Aircraft: Real-Time Application" *Journal of Intelligent & Robotic Systems*, vol. 73, pp. 137-155, 2014.

[8] N. B. Ammar, S. Bouallègue, J. Haggège, and S. Vaidyanathan., "Chattering Free Sliding Mode Controller Design for a Quadrotor Unmanned Aerial Vehicle," in *Applications of Sliding Mode Control in Science and Engineering*. Springer International Publishing, 2017.

[9] M. Zhihong and X. -H. Yu, "Terminal sliding mode control of MIMO linear systems," *IEEE Transactions on Circuits and Systems I: Fundamental Theory and Applications*, vol. 44, no. 11, pp. 1065-1070, Nov. 1997.

[10] A. M. Shotorbani, A. Ajami, S.A. Zadeh, M.P. Aghababa, and B. Mahboubi, "Robust terminal sliding mode power flow controller using unified power flow controller with adaptive observer and local measurement," *IET Generation Transmission & Distribution*, vol. 8, no. 10, pp. 1712–1723, Oct. 2014.

[11] H. Wang, et al., "Design and Implementation of Adaptive Terminal Sliding-Mode Control on a Steer-by-Wire Equipped Road Vehicle," *IEEE Transactions on Industrial Electronics*, vol. 63, no. 9, pp. 5774-5785, Sep. 2016.

[12] A. Sharafian and R. Ghasemi, "A novel terminal sliding mode observer with RBF neural network for a class of nonlinear systems," *International Journal of Systems, Control and Communications*, vol. 9, no. 4, pp. 369-385, Oct. 2018.

[13] Z. Chen, X. Yuan, X. Wu, Y. Yuan, and X. Lei. "Global fast terminal sliding mode controller for hydraulic turbine regulating system with actuator dead zone," *Journal of the Franklin Institute-engineering and Applied Mathematics*, vol. 356, no. 15, pp. 8366–8387, Sep. 2019.

[14] X. Yu and M. Zhihong, "Fast terminal sliding-mode control design for nonlinear dynamical systems," *IEEE Transactions on Circuits and Systems I: Fundamental Theory and Applications*, vol. 49, no. 2, pp. 261-264, Feb. 2002.

[15] M. G. Ghogare, S.Patil, and C. Y. Patil, "Experimental validation of optimized fast terminal sliding mode control for level system," *ISA Transactions*, vol. 126, pp. 486–497, Jun. 2022.

[16] M. C. Wu and J. C. Chen, "A Discrete-Time Global Quasi-Sliding Mode Control Scheme with Bounded External Disturbance Rejection," *Asian Journal of Control*, vol. 16, no. 6, pp. 1839–1848, Nov. 2014.

[17] C. Kadu, A. A. Khandekar, and C. Y. Patil, "Design of Sliding Mode Controller With Proportional Integral Sliding Surface for Robust Regulation and Tracking of Process Control Systems," *Journal of Dynamic Systems Measurement and Control-transactions of the Asme*, vol. 140, no. 9, Mar. 2018.

[18] J. Liu and X. Wang, *Advanced Sliding Mode Control for Mechanical Systems*. Tsinghua University Press, Beijing: Springer-Verkag Berlin Heidelberg, 2012.

[19] M. Das and C. Mahanta, "Optimal second order sliding mode control for linear uncertain systems," *ISA Transactions*, vol. 53, no. 6, pp. 1807–1815. Nov. 2014.

[20] K. Park and T. Tsuji, "Terminal sliding mode control of second-order nonlinear uncertain systems," *International Journal of Robust and Nonlinear Control*, vol. 9, no. 11, pp. 769–780, Aug. 1999.

[21] S. Yu, X. Yu, and M. Zhihong, "Robust global terminal sliding mode control of SISO nonlinear uncertain systems," in *Proceedings of the 39th IEEE Conference on Decision and Control (Cat. No.00CH37187)*, Sydney, NSW, vol. 3, 2000, pp. 2198-2203.

[22] J. J. Slotine and W. Li, *Applied non-linear control*. Englewood Cliffs, New Jersey: Prentice Hall Inc., 1991.

[23] A. Laware, D. B. Talange, and V. Bandal, "Evolutionary optimization of sliding mode controller for level control system," *ISA Transactions*, vol. 83, pp. 199–213, Dec. 2018.

[24] S. Skogestad and I. Postletwaite, *Multivariable feedback control: analysis and design*, 2nd Ed. New York: Wiley, 1996.

[25] R. Wood and M. W. Berry, "Terminal composition control of a binary distillation column," *Chemical Engineering Science*, vol. 28, no. 9, pp. 1707–1717, Sep. 1973.

[26] Q. Wang, T. H. Lee, and C. Lin, "Decentralized control: Relay feedback," *Springer*, pp. 347-373, 2003.

[27] V. D. Hajare and B. M. Patre, "Decentralized PID controller for TITO systems using characteristic ratio assignment with an experimental application," *ISA Transactions*, vol. 59, pp. 385–397, Nov. 2015.

M. G. Ghogare completed B. E. in Instrumentation Engineering in 2000 and M. E. in Instrumentation and Control Engineering in 2009. He completed his Ph.D in 2021 from College of Engineering Pune in Instrumentation and Control Engineering. His research areas include Control Systems and Signal Processing. He has published papers in International Journals and Conferences. Presently he is working as a Assistant Professor in Instrumentation Engineering department at Dr. D. Y. Patil Institute of Technology, Pune.

S. L. Patil is a Professor, Dean Alumni and International relations at College of Engineering Pune, India. He has completed his PhD from IIT Delhi in 2009. His research focuses on power electronics, power converters, power converter control, process instrumentation, biomedical instrumentation and signal processing. He has more that 28 years of teaching and research experience.

C. Y. Patil C. Y. Patil received the B.E. in Instrumentation Engineering in 1991, M.Tech. i Instrumentation and Control Engineering in 1998, and Ph.D, in 2010. He is presently working as a Professor in the Department of Instrumentation and Control at College of Engineering Pune, India. His research interests include soft computing, signals and systems and digital signal processing.

L. R. Chaudhari received the B.E. in Instrumentation Engineering from D. N. Patel College of Engineering, Shahada, Dist: Nanadurbar, Maharashtra State, India, in 1996 and M.Tech. degree from SGGS, Institute of Technology, Nanaded, Maharashtra, India in 1998. He is presently working as a Assistant Professor in the Department of Instrumentation and Control at Dr. D. Y. Patil Institute of Technology, Pimpri, Pune, India. His research interests include Process Control, Control Systems, IOT.